Cerebral Cortex April 2013;23:922–931
doi:10.1093/cercor/bhs085
Advance Access publication April 3, 2012

Early Decline in Progenitor Diversity in the Marmoset Lateral Ventricle

Kasum Azim[1], Stefan Zweifel[1], Fabienne Klaus[2], Kazuaki Yoshikawa[3], Irmgard Amrein[2] and Olivier Raineteau[1]

[1]Brain Research Institute, University of Zürich/Swiss Federal Institute of Technology Zurich (ETHZ), 8057 Zürich, Switzerland, [2]Institute of Anatomy, University of Zürich, 8057 Zürich, Switzerland and [3]Institute for Protein Research, Osaka University, Osaka 565-0871, Japan

Address correspondence to Olivier Raineteau, Brain research Institute, University of Zurich/ETHZ, Winterthurerstrasse 190, 8057 Zurich, Switzerland. Email: raineteau@hifo.uzh.ch.

The lateral ventricle (LV) of the adult rodent brain harbors neural stem cells (NSCs) that continue to generate new neurons throughout life. NSCs located in defined areas of the LV walls generate progenitors with distinct transcriptional profiles that are committed to specific neuronal fates. Here, we assessed if such diversity of NSCs also exist in the adult common marmoset, a widely used primate species in basic and clinical neuroscience research. We first investigated the 3D distributions of proliferative progenitors and committed neuroblasts in the marmoset forebrain. In addition to these maps, we assessed the spatial presence of divergent progenitor populations based on their expression of defined transcription factors, that is, Dlx2, Pax6, Tbr2, and Ngn2 which are differentially expressed by γ-aminobutyric acidergic versus glutamatergic progenitors in the adult rodent forebrain. In striking contrast to rodents, glutamatergic progenitors were only sparse in neonates and absent from the adult LV, whilst present in the hippocampus. Our analyses highlight major differences in the diversity of NSCs of the marmoset LV compared with rodents and emphasize the need to address NSCs diversity in evolutionary higher order mammals concomitantly to rodents.

Keywords: neuroblasts, neuronal lineages, primates, progenitor, subventricular zone, transcription factor

Introduction

Recent studies have considerably challenged the classical view of the presence of truly multipotent neural stem cells (NSCs) in the rodent subventricular zone (SVZ). Accumulating evidences consolidate the fact that stem cells located in subregions of the lateral ventricle (LV) contribute to the generation of distinct populations of olfactory interneurons from birth till adulthood (Kelsch et al. 2007; Merkle et al. 2007; Young et al. 2007; Fernandez et al. 2011). Furthermore, heterotopic transplantation experiments demonstrate that precursors isolated from defined SVZ subregions are restricted in capacity to generate neurons in a cell-autonomous manner (Kelsch et al. 2007; Merkle et al. 2007). In agreement with the description of a heterogeneous SVZ, transcription factors (TFs) involved in the specification of subpopulations of neurons during development maintain distinct spatial expression patterns in adult SVZ progenitors (Hack et al. 2005; Merkle et al. 2007; Brill et al. 2008, 2009). In support of their embryonic origins, markers expressed in the pallium during development such as Tbr2 persist in the dorsal SVZ and similarly subpallial markers such as Dlx2 are mainly confined to the lateral SVZ (Azim et al. submitted). These 2 populations of progenitors derive from Mash1 expressing progenitors but identify divergent lineages (Brill et al. 2009; Azim et al. submitted), that is, γ-aminobutyric acidergic (GABAergic) and Glutamatergic lineages.

Although mainly studied in rodents, adult olfactory bulb neurogenesis also occurs in various primate species, for example, marmoset (Leuner et al. 2007; Bunk et al. 2011; Sawamoto et al. 2011), squirrel monkeys (Bedard et al. 2002), and macaques (Kornack and Rakic 2001). Despite being genetically further from human, marmosets are increasingly used for studies in neurosciences because of their small size, high reproductive rate, and susceptibility to genetic engineering (Cyranoski 2009; Sasaki et al. 2009). Although the extent of proliferation and neurogenesis appears an order of magnitude lower to those observed in rodents, the longer lifespan of these animals may lead to comparable degrees of olfactory bulb neurogenesis. However, the diversity of SVZ progenitors in the primate SVZ has not yet been assessed. Here, we studied neurogenesis in the forebrain of adult common marmoset (i.e. *Callithrix jacchus*) by using not only classical markers of proliferative cells and committed neuroblasts (Ki67 and doublecortin [Dcx], respectively) but also markers of defined nonoverlapping neuronal progenitor populations.

Materials and Methods

Unless stated otherwise, all materials were obtained from Sigma-Aldrich (Buchs, CH).

Animals

In total, 6 brains of different ages of common marmoset, *C. jacchus* (M1: 31 months, M2: 32 months, M3: 32 months, M4: 56 months, M5: P0, M6: P0) were used. All adult marmosets were males and whilst both newborns were females. All animal experimentation was performed in agreement with Canton of Zurich veterinary office guidelines.

Tissue Processing

Animals were euthanized with Ketamin (10 mg/kg body weight) and Xylazine (0.5 mg/kg body weight) and perfused with heparinized phosphate buffered saline (PBS), followed by 0.6% sodium sulfide and cold 4% paraformaldehyde with 15% saturated picric acid in 0.1 M PB. Brains were removed and postfixed for 24 h in 4% paraformaldehyde. Left hemispheres were cryoprotected in 30% sucrose, and 40 μm coronal sections were collected in cryoprotection solution and stored at −20 °C until further processing. For 3D reconstruction, right hemispheres were dehydrated in alcohol and embedded in 2-hydroxyethyl-methacrylate (Kulzer GmbH & Co., Wehrheim, Germany) according to the manufacturer's instructions. Coronal sections (20 μm) were mounted and stained with a modified Nissl stain (Giemsa stock solution 1.09204.0500, Merck, Germany) diluted 1:10 in buffer (67 mM KH2PO4) at 60 °C for 10 min, rinsed in buffer for 1 min and differentiated in 3× 99% alcohol, cleared in Xylol, and mounted with Eukitt.

Immunohistochemistry

For diaminobenzidine (DAB) staining, sections were washed with PB and permeabilized by incubation in PB and 1% Triton X-100 at room temperature (RT) for 30 min. Antigen retrieval was performed with citrate buffer (10 mM $C_6H_8O_7$; pH 6) at 80 °C for 20 min to 1 h depending on age of animal. Endogenous peroxidase activity was blocked by incubation in 0.6% H_2O_2 in Tris-buffered saline (TBS: 84 mM Tris–HCl) for 30 min at RT and then washed in PB. Unspecific staining was prevented by blocking sections in 10% horse serum (HS) (GIBCO) diluted in PB containing 0.4% Triton X-100 (PBTx) at RT for 2 h. After extensive washes in PB, sections were incubated with primary antibodies in 5% HS-PBTx at 4 °C overnight. Primary antibodies used were: Rabbit anti-Tbr2, 1:1500 (Abcam, AB23345); Guinea pig anti-Dlx2, 1:5000 (Kuwajima et al. 2006); Mouse anti-Ki67, 1:500 (BD Pharm, 550609); Goat anti-Dcx, 1:500 (Santacruz, Sc-8066); Rabbit anti-Pax6, 1:400 (Covance, PRB278P). On the following day, sections were washed with PBTx and incubated with species-matched secondary antibodies in 5% HS-PBTx at RT for 2 h (Biotinylated antibodies, Jacksons Immunoresearch, 1:1000). DAB labeling was enhanced through incubation in ABC solution at RT for 90 min in TBS according to manufacturer's instructions (Vector Laboratories). Sections were incubated for 10 min in $NiSO_4$ and DAB (20 mg/mL). The DAB reaction was activated by incubating sections in the latter solution containing 0.005% H_2O_2, monitored under a dissecting microscope, and reaction discontinued by washing sections thoroughly in PB when staining stopped intensifying. Dehydration was done by sequential immersion of slides containing the stained sections in 70%, 80%, 100% EtOH and Xylol (20 s each) followed by a final wash in Xylol (2 min). Slides were immediately covered with Eukitt (Grale Scientific) and coverslipped.

For immunofluorescence staining, above procedures above were performed up to the secondary antibody stage without peroxidase activity blocking. Specie corresponding fluorophore conjugated secondary antibodies (all obtained from Invitrogen, 1:500 in 5% HS in PBTx) were incubated for 2 h at RT. Nuclear counterstaining was performed with 4′,6-diamidino-2-phenylindole (DAPI) or TOPRO (Invitrogen) in PB at RT for 5 min. Double staining was performed by applying a cocktail of 2 primary or secondary antibodies raised in different species simultaneously.

Double staining was performed by applying 2 primary and secondary antibodies simultaneously. For double staining in which the primary antibody was produced in the same animal, a more complex protocol was needed (Toth and Mezey 2007). Here, we first applied the first primary antibody and used a tyramide amplification kit from Invitrogen to amplify the fluorescent signal. We then microwaved the sections for 5 min in citric acid buffer, pH 6 in order to denature the first primary antibody. The second primary and secondary could then be applied with no risk of cross-reaction. Appropriate controls were performed by omitting the primary antibody from the second immunoreaction. These control sections showed no signal indicating that the secondary antibody against the second primary applied was not picking up any signal from the first primary antibody applied.

Quantification of Cell Distribution

Generation of the 3D reconstructions and quantification of the rostral–caudal distribution were compiled using the microscope ZEISS "Axioskop 2 MOT" equipped with the following objectives: 5×, 10×, 20×, and 40× (all Plan-NEOFLUAR; numerical apertures: 0.15, 0.30, 0.50, and 1.3, respectively). DAT files containing the quantification data were created with the software Neurolucida (MBF Bioscience; version 9.01). The brain border and the LVs were traced with different colored contours at a 5-fold magnification and 10-fold, respectively. Positive cells were marked with virtual markers at 20- and 40-fold magnifications. Each quantified section was overlaid with the previous section. Data were extracted with the software Neurolucida Explorer (MBF Bioscience; version 9.10.1) and analyzed with Excel (Microsoft; version 2007).

For examining marker or colocalization, confocal stacks compromising the entire thickness of stained sections were obtained with a LEICA SPEII or SP5 confocal microscope at a 40-fold magnification (HCX PL APO; numerical apertures: 1.25–0.75) and the software "LAS" (Leica Microsystems; version 2.2.1). Acquired stacks were analyzed with the software "Imaris x64" (Bitplane AG; version 6.4.0) and the data edited with "Excel" (Microsoft; version 2007).

Image Analysis

Images of DAB staining were produced using the upright ZEISS "Axioskop 2 MOT" microscope and the software "Neurolucida 9.01." Mosaic overviews of fluorescence staining were acquired on an epifluorescence microscope "LEICA DM5500 B" equipped with a motorized stage. SVZ overviews were acquired using a 20× objective (HCX PL FLUOTAR; numerical aperture: 0.50). Confocal micrographs were acquired using 40× (HCX PL APO; numerical aperture: 1.25–0.75) and 63× (PL APO; numerical aperture: 1.40) objectives. Higher resolution images were acquired using the "LEICA SPEII" confocal microscope at 40× and 100× (HCX PL APO; numerical apertures: 1.25–0.75 and 1.40–0.70). For both Leica microscopes, the LAS software (Leica Microsystems, version 2.2.1) was used to extract and process images that were assembled using Adobe Photoshop CS3.

Results

Serial sections from 4 adult marmosets were analyzed (i.e., 31, 32, 32, and 56 months of age). First, a 3D representation of the forebrain was performed from serial sections (20 μm sections, 1/6, Nissl stain), onto which contours of the rostral migratory path and LV, identified by the presence of Dcx and/or Ki67+ cells were superimposed. This virtual representation underlined major differences with the organization of the SVZ and rostral migratory stream (RMS) in rodents. The LV showed a complex organization, spreading 4.35 mm in the rostrocaudal axis before the emergence of the third ventricle and extending for a maximum of 4.8 mm in its ventrodorsal dimensions, representing a surface of 14.5 mm^2 (Fig. 1*A–C*). Openings (lumen) were only observed in some regions of the LV, while other regions (i.e., dorsal regions) consisted of tightly packed ependymal cells in direct opposition with each other.

Immunostaining for the proliferative marker Ki67 (Fig. 2) as well as for the committed neuroblast marker Dcx (Fig. 3) was performed in parallel on serial sections (40 μm sections, 1/10) spreading the entire forebrain from the olfactory bulb until the appearance of the third ventricle. Within the 4 adult marmosets, counts for both markers showed large interindividual variability but a clear correlation in between the animal age and cell numbers, with the youngest animal showing the most cells (i.e., 647 Ki67+ and 1687 Dcx+ cells), whilst the oldest showed considerably less cells (i.e., 85 Ki67+ and 283 Dcx+ cells). Analysis of the rostrocaudal distribution of Ki67+ cells (Fig. 2*A*,*B*) and Dcx+ cells (Fig. 3*A*,*B*) revealed that neurogenesis was clearly enriched in a relatively rostral subregion of the LV (i.e., from ~0.8 to 2.4 mm of the opening of the LV). Thus, 71.5 ± 10.2% and 80.2 ± 1.6% of Dcx+ and Ki67+ cells, respectively, were observed over 1.6 mm of the LV in the 3 younger marmosets, whereas the older marmoset showed a diffuse homogenous distribution of the cells (gray boxes in Figs 2*B* and 3*B*). Careful analysis of Ki67 and Dcx staining allowed the visualization of the RMS emerging at a very ventral location, 1.2 mm caudal to the aperture of the LV (Fig. 2*A*, arrow). Bipolar Dcx-positive cells could be identified, migrating along the nucleus accumbens toward the olfactory peduncle. Interestingly, their numbers were sparse, and chains of cells were rarely observed suggesting a reduced migratory phenotype of newborn neurons in marmosets, when compared with rodents. Only rare Dcx-positive cells were observed in the RMS and olfactory bulb (OB) (<2 cells per section). In parallel to this

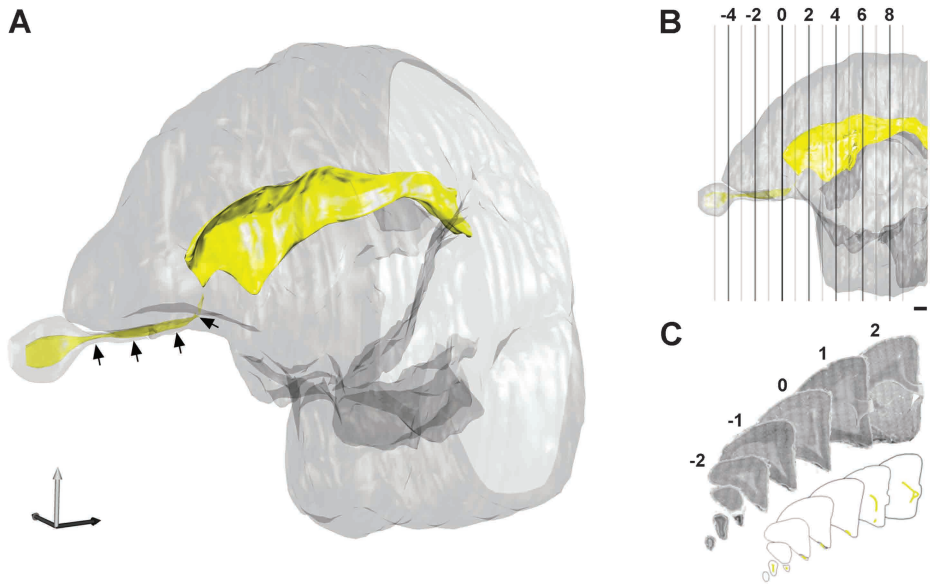

Figure 1. 3D visualization of the adult marmoset forebrain: (*A*) 3D reconstruction of serial (20 μm, ¼ section, as shown in *B*) coronal sections of a 31-month-old adult forebrain (light gray) counterstained with cresyl violet, allowing the visualization of the ventricular system (yellow). The localization of the RMS (arrowheads, yellow) is based onto the localization of cells expressing the proliferative marker Ki67 or migrating neuroblast marker Dcx. (*C*) Indication of coordinates according to the aperture of the LV, defined here as 0. The LV extends on a total of 4 mm before opening of the third ventricle.

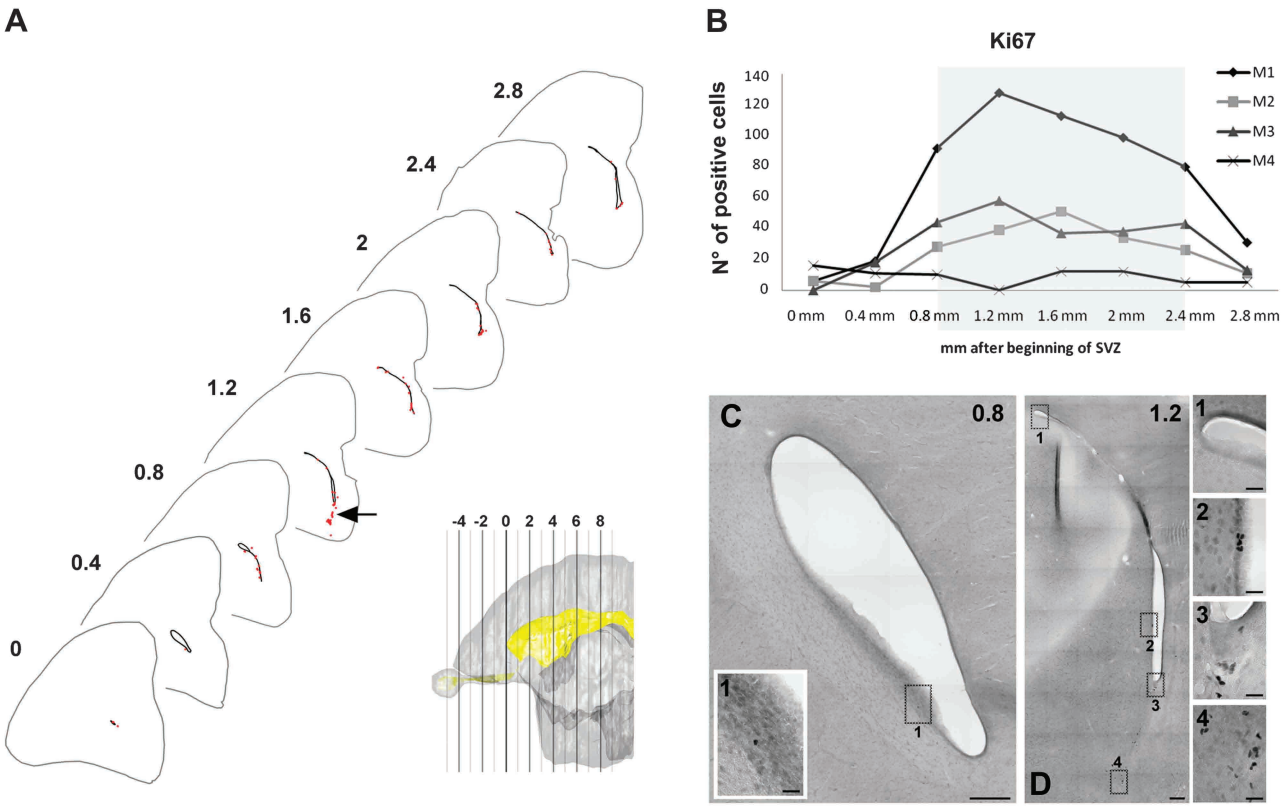

Figure 2. Spatial distribution of cycling progenitors in the LV of the adult marmoset forebrain. (*A*) Examples of virtual slices at defined rostrocaudal axis points relative to the aperture of the LV (black), illustrating the distribution of proliferative progenitors (KI67+). Only sections of the first 2.8 mm of LV are represented. RMS emerges from the ventral extremity of the LV, as indicated by an arrow at position 1.2. Proliferating cells (Ki67+, *B*) were quantified at defined rostrocaudal axis points relative to the aperture of the LV of 4 different animals of varying ages. (*C* and *D*) Examples of sections at positions 0.8 and 1.2 (according to the aperture of the LV), including captions, showing examples of Ki67+ cells. Scale bars: overview = 150 μm; captions = 50 μm.

reduced rostral migration, many Dcx+ cells (16.7 ± 4.8% of all Dcx+ cells; Fig. 3*D–H*) could be detected migrating into the striatum, with their relative proportion increasing with age (Fig. 3*F*). Many of these cells observed at distances of >200 microns from the LV showed ramified morphologies and were often associated in close proximity to blood vessels (Fig. 3*G–J*).

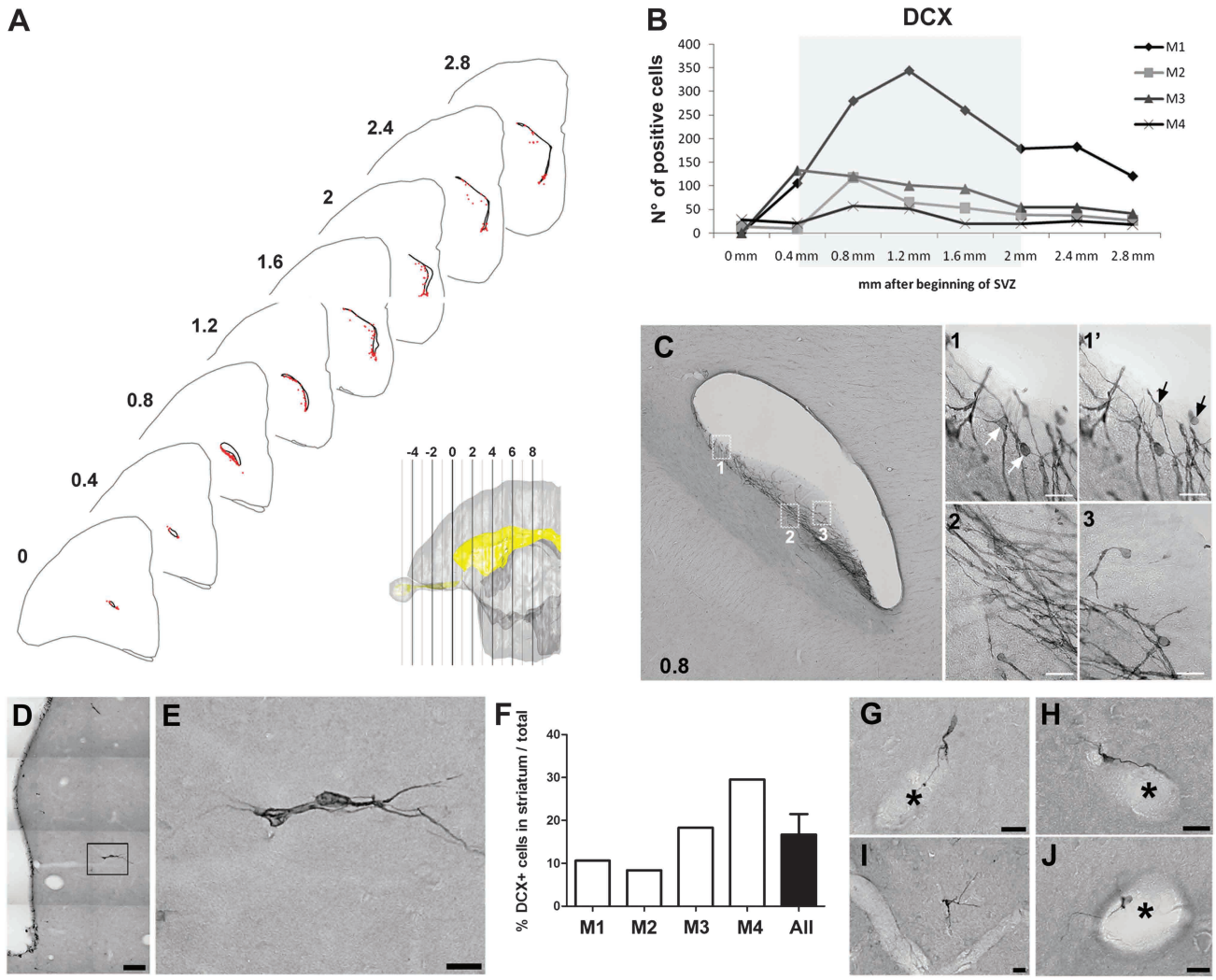

Figure 3. Spatial distribution of neuroblasts in the LV and adjacent striatum of the adult marmoset. (*A*) Examples of virtual slices at defined rostrocaudal axis points relative to the aperture of the LV (black), illustrating the distribution of neuroblasts (Dcx+, right). Only sections of the first 2.8 mm of LV are represented. (*B*) Neuroblasts (Dcx+) were quantified at defined rostrocaudal axis points relative to the aperture of the LV of 4 different animals of varying ages. (*C*) Examples of a section (0.8 caudal to the aperture of the LV) including captions showing examples of Dcx+ cells. (*D*–*H*) Neuroblasts were often observed in the striatum in adult marmosets, at some distance from the LV (*D*, *E*). Quantification of the number of striatal Dcx+ cells demonstrate their gradual accumulation with age (*F*). These Dcx+ cells often showed ramified morphologies (*I*) and were often associated with blood vessels (*G*, *H*, *J*). Scale bars: overview = 150 μm; captions = 50 μm in *C* and 20 μm in *E*–*J*.

We next addressed the diversity of SVZ progenitors by investigating the presence and distribution of progenitors showing distinct transcriptional profiles. We selected Tbr2 and Dlx2 as 2 TFs that show nonoverlapping patterns of expression in the mouse forebrain and participate in the generation of Glutamatergic and GABAergic neurons during development (Winpenny et al. 2011) as well as into adulthood (Brill et al. 2008, 2009). Immunodetection of Dlx2 revealed a large number of cells in the LV expressing high level of this protein (i.e., Dlx2 high) often grouped in clusters, while some surrounding cells expressed lower levels (Fig. 4*A*). High expressing Dlx2+ cells showed a rostrocaudal and dorsoventral spatial distribution similar to those observed for Ki67 and Dcx (Fig. 4*A*,*B*). Similarly to rodents (Brill et al. 2008), a population of Dlx2+ cells was proliferative and expressed Ki67 (Fig. 4*D*; 19.4 ± 7.1%; n = 844 Dlx2+ cells), while 59.3 ± 9.2% Dlx2+ cells expressed the committed neuroblasts marker Dcx (Fig. 4*E*; n = 476 Dlx2+ cells). Notably, the intensity of Dlx2 expression was higher in proliferating cells located in the SVZ and decreased progressively in migrating progenitors (cf. Fig. 4*D*,*E*).

In rodents, Dlx2 acts together with the other homeodomain TF Pax6 to specify subtypes of olfactory bulb GABAergic neurons (Brill et al. 2008). We therefore investigated the expression of Pax6 and its interrelation with Dlx2 in the marmoset LV. Many cells could be observed to express Pax6 in the ependymal, subependymal, and overlying parenchyma. Only a small population of subependymal cells were proliferative 3.1 ± 0.7% (n = 2562 Pax6+ cells), while 1.8 ± 1.1% expressed the neuroblasts marker Dcx (n = 1343 Pax6+ cells). Because of the widespread expression of Pax6 in various cell types, our analysis was focused on progenitor cells, that is, proliferative cells that express the mitotic factor Ki67. These analysis revealed that 39.7 ± 16.4% of Ki67+ proliferating progenitors expressed Pax6 (n = 219 Ki67+ cells) and 62.0 ± 6.0% expressed Dlx2 (n = 143 Ki67+ cells). These results suggest a mutually exclusive expression of Pax6 or Dlx2 by divergent populations of progenitor cells. To address this

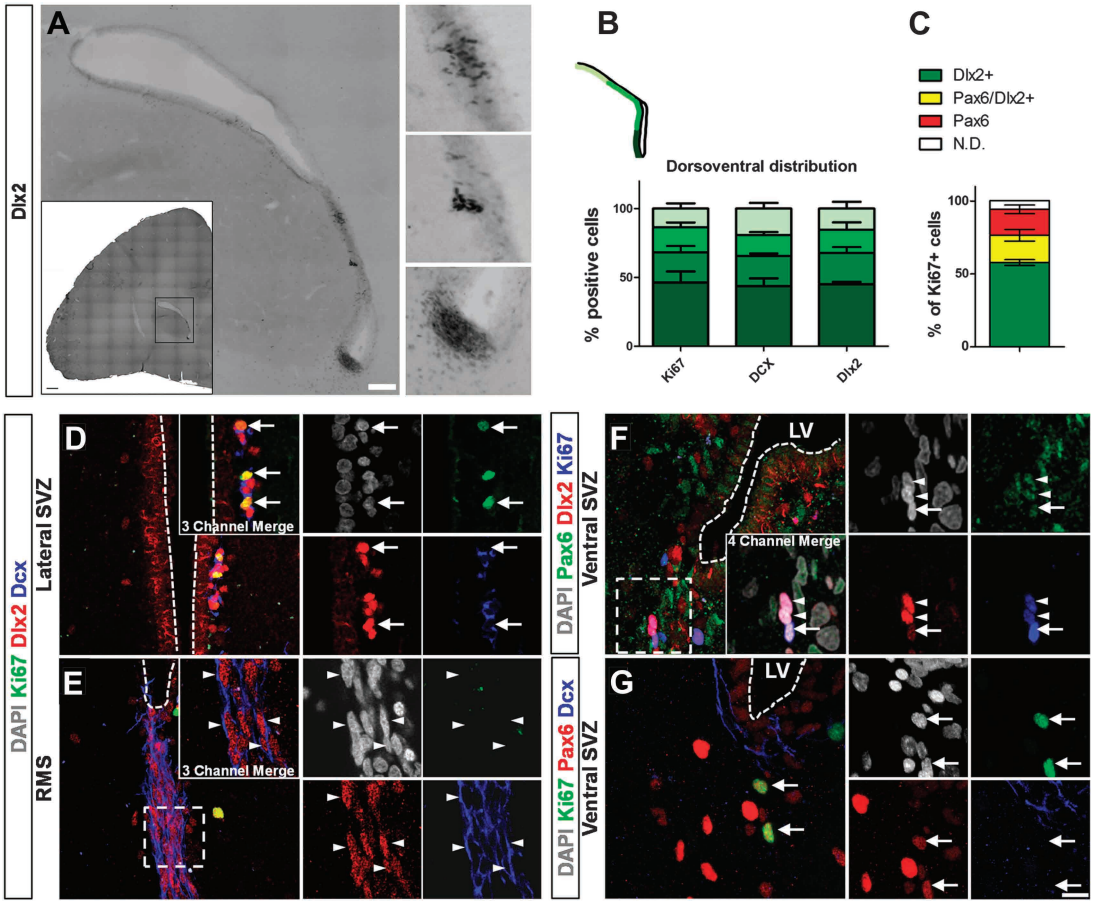

Figure 4. Distribution of Dlx2+ progenitors in the LV of the adult marmoset forebrain. (*A*) Example of a rostral coronal section, including captions and crops, showing examples of Dlx2+ progenitors in the lateral and ventral SVZ where staining is concerted (see captions of *A*). (*B*) Histogram showing the dorsoventral distribution of cells expressing Ki67, Dcx, and Dlx2 in 4 equal dorsoventral regions of the LV (defined as shades of green in left schematic drawing). Note the similar distribution of cells expressing the 3 markers, suggesting homogeneous distribution of Dlx2 progenitors. (*C*) Histogram showing the expression of Dlx2 (green), pax6 (red), or both (yellow) in proliferative Ki67+ cells of the SVZ. (*D–E*) Overview and higher magnification images illustrating the immunoreactivity of Dlx2+ cells for Ki67 (*D*) and Dcx (*E*). Arrow shows examples of Dlx2+/Ki67+/Dcx− progenitors, whilst arrowheads shows examples of Ki67−/Dlx2+/Dcx+ neuroblasts. Dotted lines indicate approximately the ventricular space. (*F–G*) Numerous Pax6+ cells could be observed in all regions of the LV. Some Pax6+ cells coexpress Ki67 (arrows, *F–G*) and of these were frequently positive for Dlx2 (arrowheads, *F*) although not Dcx (*G*). Overviews in *C–F* are flattened maximum intensity projections of 15–18 μm thickness. Higher magnification images are single focal planes. Scale bars: *A* = 100 μm; *C–E* (overview) = 20 μm, *C–E* (inserts) = 10 μm. *G* overview and captions = 15 μm.

more directly, we performed triple staining for Ki67, Pax6, and Dlx2 and compared the pattern of expression and overlap in between these 3 markers. Our result shows that 18.8 ± 4% of Ki67+ proliferating progenitors (n = 125) expressed both Pax6 and Dlx2 (i.e., triple positive); while 17.4 ± 0.8% expressed Pax6 and 57.8 ± 3.4% expressed Dlx2 only. These results indicate the coexistence of 3 populations of progenitors, that is, one that express both TFs, one expressing Pax6 only, and a larger one Dlx2 only (i.e., double positive, Fig. 4*C*). Interestingly, about half of the Pax6/Dlx2 double-positive cells expressed Ki67 (51.1 ± 2.0%, n = 125 Ki67+ cells) illustrating that this combination of marker is often associated, but not exclusively, with proliferation (Fig. 4*F,G*). These results therefore support that proliferative progenitors of the marmoset LV are heterogeneous in regard to Pax6 and Dlx2 expression, as previously observed in rodents (Brill et al. 2008).

To further explore the heterogeneity of progenitors in the marmoset LV, we next assessed expression of the T-box TF Tbr2 (Fig. 5). Notably, no Tbr2 expression could be observed in any regions of the LV of the adult marmosets (Fig. 5*A,B*). Intensive Tbr2 staining was, however, observed in the olfactory bulb of all marmosets (Fig. 5*C*), discarding a failure in the immunodetection of this antigen. Here, Tbr2+ cells were distributed in the mitral and periglomerular cell layer, as previously described in the mouse (Winpenny et al. 2011) (Fig. 5*C,D*). This population of Tbr2+ neurons was negative for Dlx2+ (n = 471 Tbr2+ cells), a marker of GABAergic periglomerular interneurons in rodents (Brill et al. 2008). Furthermore, expression of Tbr2 was confirmed in progenitors of glutamatergic neuron progenitors in the dentate gyrus of the same animals, a region that continues producing glutamatergic granule cells throughout life (Leuner et al. 2007) (Fig. 5*E–G*). Similarly to mice, 18% Tbr2+ cells were proliferative (n = 55 Tbr2+ cells), while 47% Tbr2+ cells expressed the neuroblasts marker Dcx (n = 55 Tbr2+ cells; Fig. 5*F,G*). Furthermore, Tbr2+ progenitors coexpressed Pax6 (i.e., 60% n = 45 cells, Fig. 5*G*), a marker of stem cells and progenitor in rodents (Maekawa et al. 2005; Nacher et al. 2005), verifying expression of Tbr2 in early progenitor cells as shown in rodents (Hodge et al. 2008). This is further supported by the expression of the proliferative marker Ki67 in a significant proportion of Pax6/Tbr2 double-positive cells (28.9%; n = 45 cells; Fig. 5*G*).

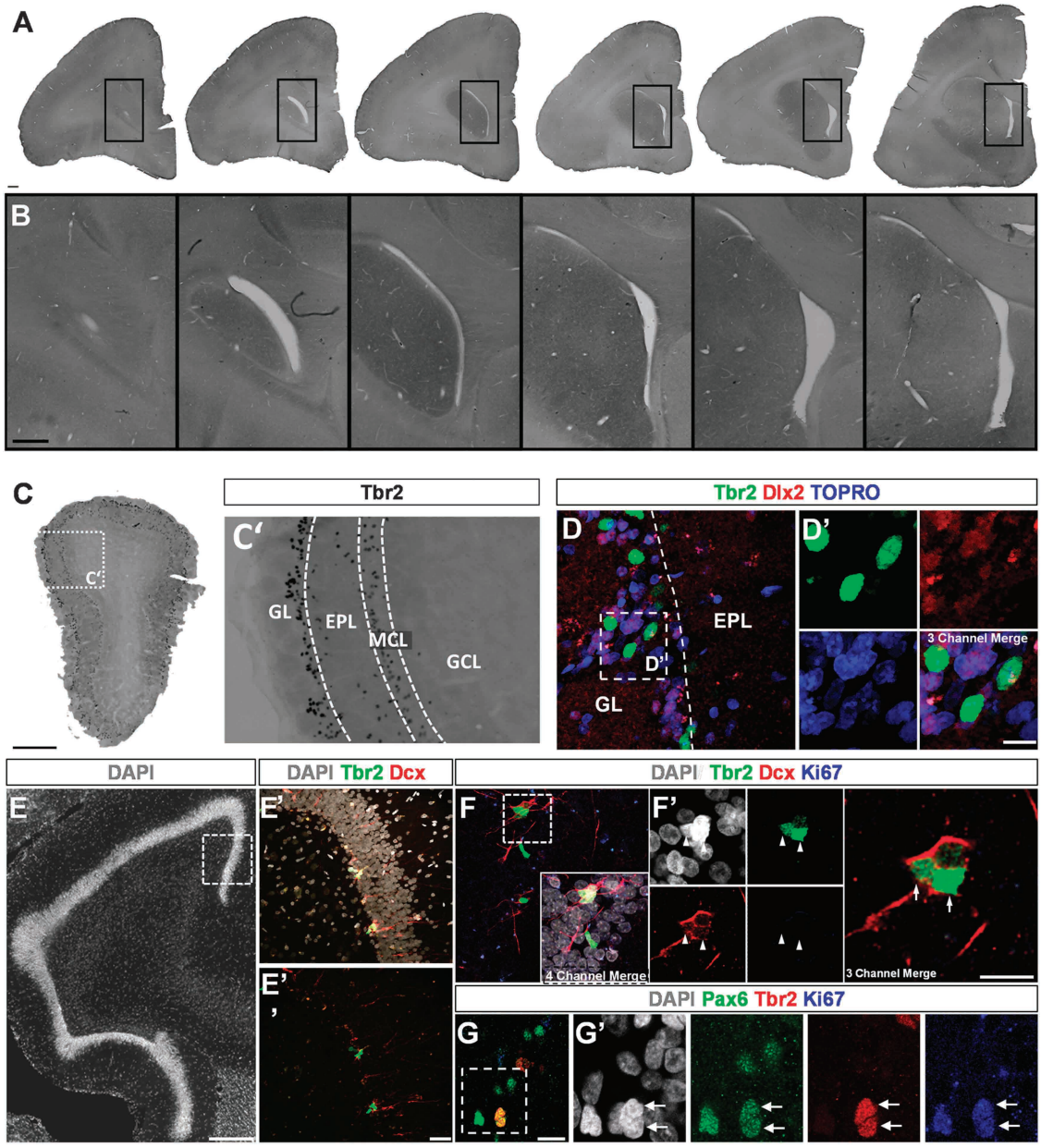

Figure 5. Tbr2+ progenitors are absent from the adult marmoset LV but are present in regions of adult glutamatergic neurogenesis. (*A*) Representative overviews of the LV in coronal sections of the anterior LV illustrating the absence of Tbr2+ cells (corresponding higher magnification images of the LV are shown in *B*). (*C*) Representative overview and higher magnification of the olfactory bulb of the same animal, confirming immunodetection of Tbr2 in the mitral cell, external plexiform, and glomerular cell layers. (*D*) Absence of colocalization of large Tbr2+ (green) and smaller Dlx2+ (red) cells in the periglomerular cell layer, visualized by TOPRO counterstain (blue). Right panels show higher magnification of boxes in *D*. All panels are flattened maximum intensity projections of 18 μm thickness. (*E*–*G*) Tbr2 is expressed in progenitors of glutamatergic granule cells in the adult marmoset hippocampus. (*E*) Overview of DAPI stained fluorescent micrograph illustrating the structure of the rostral dentate gyrus. (*E′*, *E″*) Flattened confocal micrographs show an example of Tbr2+ cell clusters and Dcx+ neuroblasts that are expanded from the dotted box of *E*. (*F*, *F′*) High magnification photomicrographs of a cluster of Tbr2+ cells colocalizing with Dcx and negative for the proliferation marker Ki67. (*G*, *G′*) Similarly to rodents, numerous Pax6+ cells are present in germinal regions of the hippocampus. Tbr2 often colocalized with Pax6 and Ki67 (arrows), supporting its expression in early progenitors of glutamatergic granule cells. Overviews in *D*–*G* are flattened maximum intensity projections of 15–18 μm thickness, higher magnification images are single focal planes. Scale bars: *A*–*B* = 500 μm; *C* = 100 μm, *D*–*G* (overviews) = 20 μm; *D*–*G* (inserts) = 10 μm GL: Glomerular layer, EPL: External plexiform layer, MCL: Mitral cell layer, GCL: Granule cell layer.

We next investigated if these observations reflected an early loss of Tbr2+ progenitors. Neonatal marmoset forebrain sections were immunostained for Ki67, Dcx, as well as for Tbr2 and Dlx2 (Fig. 6). As characterized already in other monkey species (Leuner et al. 2007), the number of proliferating cells and neuroblasts migrating as clear neuronal chains was considerably higher than at adult stages (Fig. 6*B*). Again, although many Dlx2+ cells were observed, 18.3 ± 3.8% of which colocalized with Ki67 (n = 201 of 1077 Dlx2+ cells) and 43.4 ± 3.7% colocalized with Dcx (n = 476 of 1086 Dlx2+ cells), only rare Tbr2+ cells were observed (<20 cells per animal) in the SVZ per rostral section which had the maximal numbers. Cells positive for the 2 markers were largely spatially separated, with Tbr2+ cells present in the dorsal-most regions of the LV lateral wall, while most Dlx2+ cells were observed in the lateral and ventral regions (Fig. 6*A*, cf. insert 3 to inserts 4–6). In the dorsolateral

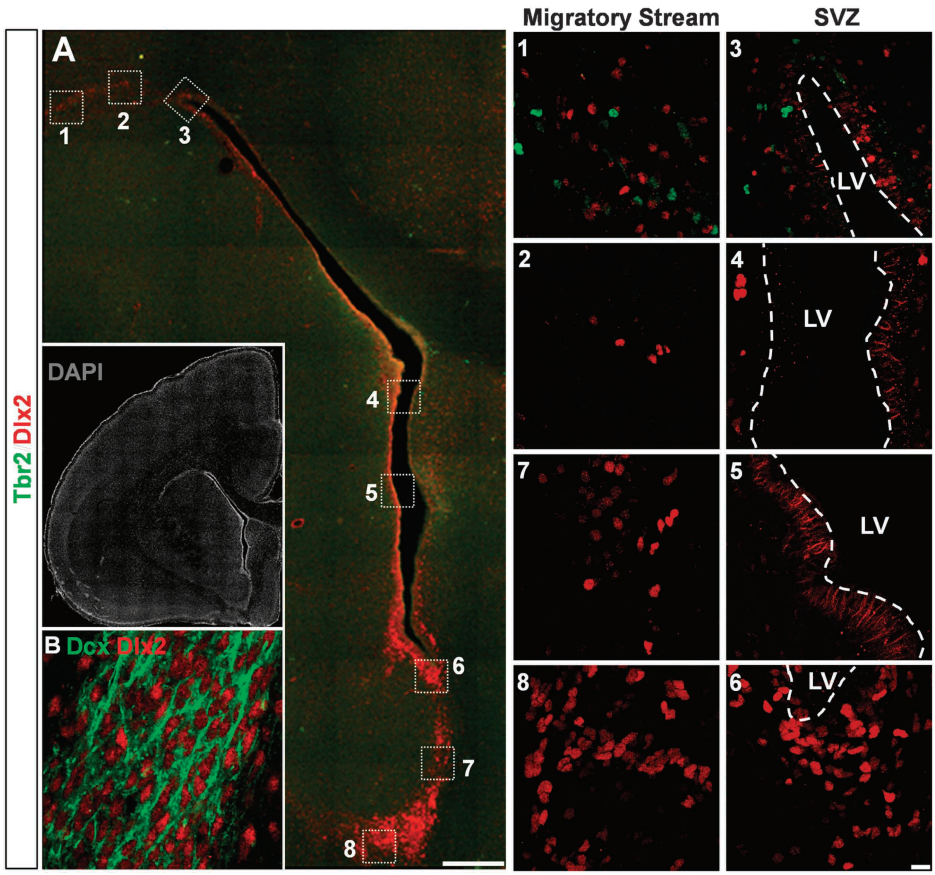

Figure 6. Dlx2 and Tbr2 identify distinct populations of SVZ progenitors in the LV of the neonatal marmoset. (*A*) Overview of Tbr2 (green) and Dlx2 (red) expressing cells in the LV of the neonatal marmoset forebrain illustrated at position 1.6 mm of the aperture of the LV. Insert shows an overview of the section counterstained with DAPI. (1–8) Captions of the lateral wall, medial wall, and migratory stream, respectively, as indicated by the boxes shown in *A*. Tbr2+ cells are only observed at the dorsal edge of the LV SVZ (2 and 5). Dlx2+ cells are observed in greater densities throughout the ventral, lateral, and dorsal SVZ of the LV (1–8). Dotted lines mark the position of the ventricular lumen. Captions 1–8 are flattened confocal *z*-sections of 15 μm thickness. Dotted lines indicate the ventricular space. (*B*) Flattened maximal intensity projection of 18 μm thickness illustrating the expression of Dcx by most Dlx2+ cells in the RMS. Scale bars: overview = 250 μm; inserts = 15 μm.

region of the LV, where both Dlx2+ and Tbr2+ cells were observed, no colocalization was ever apparent in several sections per animal studied (n = 260 Tbr2+ and n = 970 Dlx2 cells). Analysis of several rostral sections per animal, 34.4 ± 2.3% Tbr2+ cells were proliferative (i.e., Ki67+, n = 200 cells, Fig. 7*A*), while 13.9 ± 10.6% expressed the neuroblasts marker Dcx (n = 78 cells). The numbers of Tbr2+ versus Dlx2+ expressing cells in the SVZ were fractional (1.9%) only in the 2 neonatal animals studied. Thus, these analyses implicate spatially separate and defined nonoverlapping lineages, with Dlx2+ progenitor numbers far outweighing those of the Tbr2+ lineages.

In mouse, throughout different developmental windows, in the SVZ, Tbr2+ progenitors are derived from Ngn2+ progenitors (Brill et al. 2009; Winpenny et al. 2011). We therefore investigated whether the low numbers of Tbr2+ progenitors are due to lack of upstream molecular cues by examining Ngn2 expression in the neonate SVZ. In comparison with Tbr2+ progenitors that were already low in density against Dlx2+ progenitors, Ngn2+ expressing cell that colocalized with Tbr2 and Ki67, could be observed in the hippocampus (data not shown) as well as dorsal SVZ (Fig. 7*A*). The numbers of Ngn2 expressing progenitors were lower than those of Tbr2, but frequent colocalization was observed in between the 2 markers. Virtually, all of the few Ngn2+ cells observed in the dorsal SVZ were Tbr2+, and 15% (±3.4% SD) of Tbr2+ cells were positive for Ngn2 (Fig. 7*B*). In age-matched mouse, we evidence that Tbr2-expressing cells are abundant in the dorsal SVZ (Fig. 7*A*) and overlap considerably with Ngn2 (Fig. 7*B*). The complete dorsoventral span of the neonatal mouse LV was examined for Dlx2- and Tbr2-expressing progenitors for quantification and comparison with the neonatal marmoset (Fig. 7*D*). In mouse, Tbr2+ progenitors were 17.2% compared with Dlx2+ progenitors. Thus, while aged-matched mouse contained approximately 5-folds the numbers of Dlx2+ progenitors observed in marmoset, neonatal mouse contained nearly 50-folds greater Tbr2+ progenitors. These observations imply that the loss of progenitor diversity from the adult LV is already apparent at birth in the marmoset.

Discussion

Evidence of neurogenesis in the SVZ of primates is relatively sparse compared with rodents. Information on the rostrocaudal dissemination of progenitors of defined neuronal lineages has not yet been studied. Here, we mapped the locations of proliferating cells and neuroblasts in periventricular sections containing the LV and the RMS and studied nonoverlapping markers of progenitors for GABAergic and glutamatergic neurons. Our results support the existence of a regional heterogeneity of SVZ stem and progenitor cells, similar to

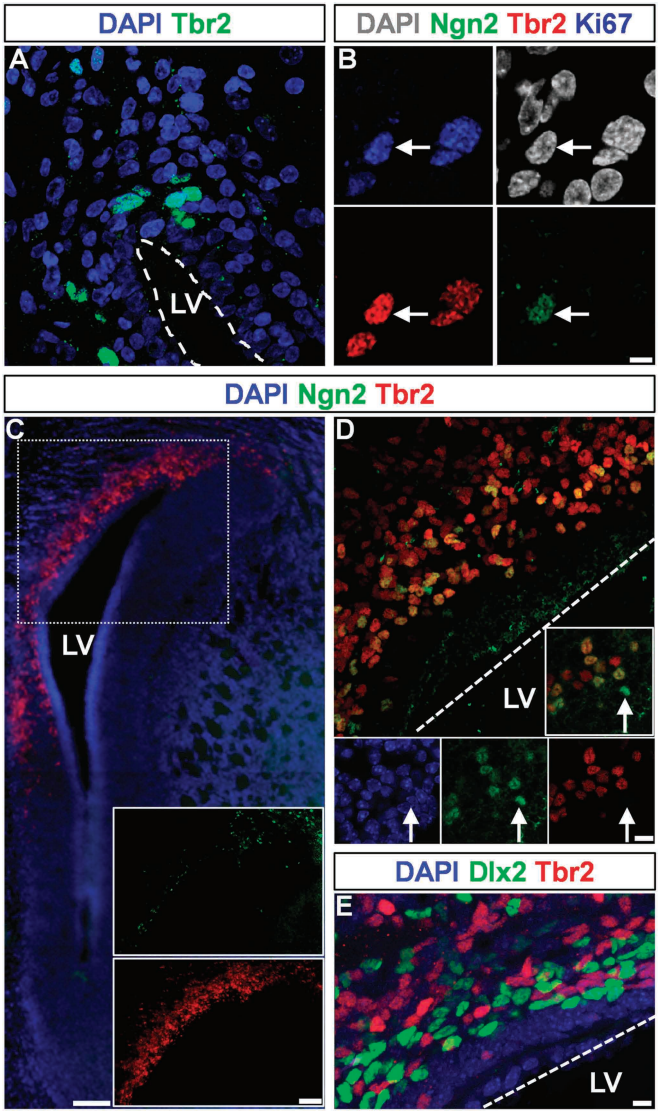

Figure 7. Sparse expression of Tbr2 and Ngn2 in progenitors of the neonatal marmoset LV. (*A*) Maximal intensity projection showing Tbr2+ progenitors in the dorsal most aspect of the LV. (*B*) Tbr2+ progenitor positive for Ngn2 and Ki67 (arrow) in the same region. (*C*) Overviews showing the expression and overlap of Tbr2+ and Ngn2+ cells in the neonatal mouse forebrain, for comparative purposes. (*D*) Overview, single confocal plane insert and captions at higher magnification of the same region show numerous Ngn2+/Tbr+ progenitors showing largely overlapping expression and arrow shows Ngn2+/Tbr2− progenitor. (*E*) The dorsal SVZ of P2 mouse rostral sections containing the LV were immunolabelled for Dlx2 (green) and Tbr2 (red) and counterstained with DAPI to illustrate the high density of these progenitor types. Dotted lines indicate approximately the ventricular space. Flattened maximal intensity projections of *A* and *D* are of 15 μm depth and *E* of 10 μm depth. Scale bar: *B* = 10 μm and 15 μm in *A*; *C* = 100 μm for overview and inserts, *D* = 20 μm in overview and 15 μm in insert or captions; *E* = 10 μm.

rodents. This heterogeneity is, however, only observed during early postnatal life. In the adult marmoset LV, the loss of Tbr2-positive progenitors associated with the widespread expression of Dlx2, suggests an early and dramatic decline in the diversity of SVZ progenitors.

Our analysis of Ki67- and Dcx-positive cells in serial sections of the marmoset LV provides a complete spatial mapping of proliferating progenitors and neuroblasts, respectively. As previously reported in mice, greater frequencies in proliferating cells or neuroblasts are apparent in rostral periventricular sections than caudal ones (Golmohammadi et al. 2008; Azim et al. submitted). The flow of the cerebral spinal fluid, which contains several morphogens and growth factors, is likely to be instrumental to the establishment of this polarity (Sawamoto et al. 2006; Bunk et al. 2011; Lehtinen et al. 2011). Our reconstructions also illustrate the ventral origin of the RMS both in neonate animals but also in the adult (McDermott and Lantos 1990; Bunk et al. 2011; Sawamoto et al. 2011), with chains of migrating neuroblasts only evident in regions approximately 1.2 mm caudal to the aperture of the LV, similarly to the reported RMS in the rhesus monkey (Pencea et al. 2001) and human forebrain (Sanai et al. 2011).

In agreement with previous primate studies and despite large interindividual variability that are likely to reflect the outbred nature of this specie, our quantifications show a dramatic decline in the number of proliferative cells and migrating neuroblasts in marmosets compared with rodents (Bunk et al. 2011), as well as from birth to adulthood (Leuner et al. 2007). The findings that few proliferating cells are present in the SVZ compared with the RMS and the mode of neuroblast migration in brain sections containing the RMS or olfactory peduncle appear to be conserved as in other monkey species such as the rhesus monkey (Pencea et al. 2001), macaque (Kornack and Rakic 2001), and squirrel monkey (Bedard et al. 2002). This decline is also observed in humans (Sanai et al. 2011), correlates with a rapid and almost completes disappearance of the RMS (Bunk et al. 2011; Sanai et al. 2011; Sawamoto et al. 2011). We describe here, that this decline could be paralleled by an increasing number of neuroblasts migrating in the striatum. They represented as much as 30% of all Dcx+ cells quantified in older animals. In this region, chains of neuroblasts, as well as more differentiated ramified Dcx+ neurons, could be observed at close proximity to blood vessels. Future studies in which reasonable *n* numbers of primates at similar time points are analyzed could shed light on this, including the interindividual variability in studied markers. Apposition of neuroblasts to blood vessels has been reported in mice both in the intact or injured forebrain and is believed to reflect trophic support by the growth factors such as brain derived neurotrophic factor (BDNF) (Snapyan et al. 2009; Whitman and Greer 2009). In agreement, viral BDNF delivered in squirrel monkey increases the number of striatal neurons exhibiting the chemical phenotype of medium spiny neurons (Bedard et al. 2006).

Our analysis of the pattern of expression of TF expressed in divergent lineages support the existence of a reduced regional heterogeneity of SVZ stem and progenitor cells in adult primates when compared with rodents. In rodents, accumulating evidence underlines major differences in the time and place of origin of OB neurons (Lledo et al. 2008; Weinandy et al. 2011), with distinct OB neuronal subtypes originating from defined subdomains of the walls of the LV, both in the early postnatal (Merkle et al. 2007; Fernandez et al. 2011) and adult forebrain (Kohwi et al. 2005; Kelsch et al. 2007; Merkle et al. 2007; Young et al. 2007; Brill et al. 2009). Defined TFs are expressed in progenitors of the LV and participate in the early specification of SVZ-NSCs toward a specific neuronal fate (Kohwi et al. 2005; Young et al. 2007; Brill et al. 2008, 2009). Here, we investigated the expression of the TF Dlx2 that has been shown to be expressed in the adult SVZ in rodents and to participate to the generation of virtually all OB interneurons (Batista-Brito et al. 2008). We also investigated the expression of Pax6, a TF that acts together with Dlx2 to specify subtypes of

olfactory bulb GABAergic neurons (Brill et al. 2008). In addition, we investigated the expression of Tbr2 (also referred to as Eomes) and Ngn2, which we have recently shown to be sequentially expressed in a subpopulation of progenitors arising from the dorsal SVZ (Brill et al. 2009; Winpenny et al. 2011), that give rise to a small population of OB glutamatergic interneurons.

Careful analysis of these markers shows a widespread partially overlapping expression of Dlx2 and Pax6. In agreement with previous observations in the mouse, Dlx2 labels a larger population of proliferating cells, while a smaller population expresses Pax6 in combination with Dlx2 or alone (Brill et al. 2008). Previous studies have suggested that the balance between Pax6 and Dlx2 expression acts as transcriptional codes for the specification of olfactory bulb periglomerular interneurons. Thus, calbindin-positive olfactory bulb interneurons would derive from progenitors expressing Dlx2 but not Pax6, while dopaminergic interneurons would derive from progenitors expressing both TFs (Allen et al. 2007; Brill et al. 2008; Weinandy et al. 2011). These observations based on Pax6 and Dlx2 expression therefore suggest that some level of progenitor diversity can still be observed in the primate. Strikingly, however, our results suggest that other lineages are absent in the marmoset LV as illustrated by the early loss of Tbr2/Ngn2 progenitors observed in this study. Our results cannot be attributed to a failure of detection of these markers, as Tbr2 could readily be observed in progenitors of glutamatergic granule cells in the dentate gyrus in all individuals, as observed in the mouse (Hodge et al. 2008). Moreover, numerous Tbr2-positive cells could be observed in the mitral cell and glomerular cell layer in the olfactory bulb. These Tbr2-positive cells were larger than the surrounding Dlx2+ cells and are likely to be glutamatergic projection and juxtaglomerular interneurons as we have recently described in the mouse (Brill et al. 2009; Winpenny et al. 2011). The similarities of the pattern of Tbr2 expression compared with rodents dismiss failure in Tbr2 detection in LV progenitors due to delayed expression. Thus, although a delay of newborn neurons maturation has recently been described in the primate DG (Kohler et al. 2011), colocalization of Tbr2 with proliferation and neuroblasts markers observed in our analysis is consistent with a timing of expression similar in mouse (Hodge et al. 2008).

Thus, our results indicate a decline of progenitor diversity in the marmoset LV that is further supported by our analysis of progenitor populations in the neonatal marmoset forebrain. At this early age, although a population of Tbr2+ progenitors could be observed in a dorsal region of the LV lateral cortical stream, in agreement with the pattern of expression in mice (Carney et al. 2006; Winpenny et al. 2011), the number of Tbr2+ progenitors at this early age was surprisingly lower than in mouse. These results were further confirmed by immunodetection of the proneural gene *Ngn2* that is expressed together with Tbr2 during glutamatergic neurogenesis (Hevner et al. 2006).

First descriptions of proliferation and/or neurogenic activity in the SVZ not only in rodents (Altman 1963), common marmosets (McDermott and Lantos 1990), macaques (Kornack and Rakic 2001; Pencea et al. 2001), squirrel monkeys (Bedard et al. 2002), and humans (Sanai et al. 2004) but also rabbits (Luzzati et al. 2003) cattle (Rodriguez-Perez et al. 2003), hedgehogs (Alpar et al. 2010), and flying foxes (Gatome et al. 2010) indicate that the neurogenic potential in the mammalian SVZ is widespread. However, there are clear species-specific differences in the organization of the SVZ and RMS, both in cellular composition and developmental changes in morphology (reviewed in detail by Bonfanti and Peretto 2011). Most obvious is the fast down-regulation of proliferation activity with age in long-lived mammals. We show here that neurogenesis in the adult marmoset forebrain is still apparent but characterized by a decline in the diversity of SVZ progenitors early in life which depict regulatory differences between primates and rodents. Importantly, this decline in the diversity of SVZ progenitors is already apparent at birth. Thus, only few Tbr2+ progenitors could be observed in the neonatal LV, and none were observed in the LV of marmosets of 2.5 years of age, corresponding to early adulthood in these animals that show an average life expectancy of 12 years (Abbott et al. 2003). These observations have important consequences for the development of stem cell–based therapies in humans (Quinones-Hinojosa et al. 2007) and emphasize that care must be taken when generalizing observations made in rodent to higher-order species.

Funding

K.A. is supported by a National Research Project (NRP63) grant from the Swiss National Fund (406340_128291). K.Y. is supported by a Grant-in-Aid for Scientific Research B2 (21300138) from the Japan Society for the Promotion of Science.

Notes

Conflict of Interest: None declared.

References

Abbott DH, Barnett DK, Colman RJ, Yamamoto ME, Schultz-Darken NJ. 2003. Aspects of common marmoset basic biology and life history important for biomedical research. Comp Med. 53:339–350.

Allen ZJ 2nd, Waclaw RR, Colbert MC, Campbell K. 2007. Molecular identity of olfactory bulb interneurons: transcriptional codes of periglomerular neuron subtypes. J Mol Histol. 38:517–525(Epub 2007 Jul 2012).

Alpar A, Kunzle H, Gartner U, Popkova Y, Bauer U, Grosche J, Reichenbach A, Hartig W. 2010. Slow age-dependent decline of doublecortin expression and BrdU labeling in the forebrain from lesser hedgehog tenrecs. Brain Res. 1330:9–19.

Altman J. 1963. Autoradiographic investigation of cell proliferation in the brains of rats and cats. Anat Rec. 145:573–591.

Azim K, Zweifel S, Yoshikawa K, Slomianka L, Raineteau O. submitted. Progenitor population locations and population sizes in the adult mouse lateral ventricle.

Batista-Brito R, Close J, Machold R, Fishell G. 2008. The distinct temporal origins of olfactory bulb interneuron subtypes. J Neurosci. 28:3966–3975.

Bedard A, Gravel C, Parent A. 2006. Chemical characterization of newly generated neurons in the striatum of adult primates. Exp Brain Res. 170:501–512.

Bedard A, Levesque M, Bernier PJ, Parent A. 2002. The rostral migratory stream in adult squirrel monkeys: contribution of new neurons to the olfactory tubercle and involvement of the antiapoptotic protein Bcl-2. Eur J Neurosci. 16:1917–1924.

Bonfanti L, Peretto P. 2011. Adult neurogenesis in mammals—a theme with many variations. Eur J Neurosci. 34:930–950.

Brill MS, Ninkovic J, Winpenny E, Hodge RD, Ozen I, Yang R, Lepier A, Gascon S, Erdelyi F, Szabo G, et al. 2009. Adult generation of glutamatergic olfactory bulb interneurons. Nat Neurosci. 12:1524–1533.

Brill MS, Snapyan M, Wohlfrom H, Ninkovic J, Jawerka M, Mastick GS, Ashery-Padan R, Saghatelyan A, Berninger B, Gotz M. 2008. A dlx2-

and pax6-dependent transcriptional code for periglomerular neuron specification in the adult olfactory bulb. J Neurosci. 28:6439–6452.
Bunk EC, Stelzer S, Hermann S, Schafers M, Schlatt S, Schwamborn JC. 2011. Cellular organization of adult neurogenesis in the Common Marmoset. Aging Cell. 10:28–38.
Carney RS, Alfonso TB, Cohen D, Dai H, Nery S, Stoica B, Slotkin J, Bregman BS, Fishell G, Corbin JG. 2006. Cell migration along the lateral cortical stream to the developing basal telencephalic limbic system. J Neurosci. 26:11562–11574.
Cyranoski D. 2009. Marmoset model takes centre stage. Nature. 459:492.
Fernandez ME, Croce S, Boutin C, Cremer H, Raineteau O. 2011. Targeted electroporation of defined lateral ventricular walls: a novel and rapid method to study fate specification during postnatal forebrain neurogenesis. Neural Dev. 6:1–12.
Gatome CW, Mwangi DK, Lipp HP, Amrein I. 2010. Hippocampal neurogenesis and cortical cellular plasticity in Wahlberg's epaulette fruit bat: a qualitative and quantitative study. Brain Behav Evol. 76:116–127.
Golmohammadi MG, Blackmore DG, Large B, Azari H, Esfandiary E, Paxinos G, Franklin KB, Reynolds BA, Rietze RL. 2008. Comparative analysis of the frequency and distribution of stem and progenitor cells in the adult mouse brain. Stem Cells. 26:979–987.
Hack MA, Saghatelyan A, de Chevigny A, Pfeifer A, Ashery-Padan R, Lledo PM, Gèotz M. 2005. Neuronal fate determinants of adult olfactory bulb neurogenesis. Nat Neurosci. 8:865–872.
Hevner RF, Hodge RD, Daza RA, Englund C. 2006. Transcription factors in glutamatergic neurogenesis: conserved programs in neocortex, cerebellum, and adult hippocampus. Neurosci Res. 55:223–233.
Hodge RD, Kowalczyk TD, Wolf SA, Encinas JM, Rippey C, Enikolopov G, Kempermann G, Hevner RF. 2008. Intermediate progenitors in adult hippocampal neurogenesis: Tbr2 expression and coordinate regulation of neuronal output. J Neurosci. 28:3707–3717.
Kelsch W, Mosley CP, Lin CW, Lois C. 2007. Distinct mammalian precursors are committed to generate neurons with defined dendritic projection patterns. PLoS Biol. 5:e300.
Kohler SJ, Williams NI, Stanton GB, Cameron JL, Greenough WT. 2011. Maturation time of new granule cells in the dentate gyrus of adult macaque monkeys exceeds six months. Proc Natl Acad Sci U S A. 108:10326–10331.
Kohwi M, Osumi N, Rubenstein JL, Alvarez-Buylla A. 2005. Pax6 is required for making specific subpopulations of granule and periglomerular neurons in the olfactory bulb. J Neurosci. 25:6997–7003.
Kornack DR, Rakic P. 2001. The generation, migration, and differentiation of olfactory neurons in the adult primate brain. Proc Natl Acad Sci U S A. 98:4752–4757.
Kuwajima T, Nishimura I, Yoshikawa K. 2006. Necdin promotes GABAergic neuron differentiation in cooperation with Dlx homeodomain proteins. J Neurosci. 26:5383–5392.
Lehtinen MK, Zappaterra MW, Chen X, Yang YJ, Hill AD, Lun M, Maynard T, Gonzalez D, Kim S, Ye P, et al. 2011. The cerebrospinal fluid provides a proliferative niche for neural progenitor cells. Neuron. 69:893–905.
Leuner B, Kozorovitskiy Y, Gross CG, Gould E. 2007. Diminished adult neurogenesis in the marmoset brain precedes old age. Proc Natl Acad Sci U S A. 104:17169–17173.
Lledo PM, Merkle FT, Alvarez-Buylla A. 2008. Origin and function of olfactory bulb interneuron diversity. Trends Neurosci. 31:392–400.
Luzzati F, Peretto P, Aimar P, Ponti G, Fasolo A, Bonfanti L. 2003. Glia-independent chains of neuroblasts through the subcortical parenchyma of the adult rabbit brain. Proc Natl Acad Sci U S A. 100:13036–13041.
Maekawa M, Takashima N, Arai Y, Nomura T, Inokuchi K, Yuasa S, Osumi N. 2005. Pax6 is required for production and maintenance of progenitor cells in postnatal hippocampal neurogenesis. Genes Cells. 10:1001–1014.
McDermott KW, Lantos PL. 1990. Cell proliferation in the subependymal layer of the postnatal marmoset, Callithrix jacchus. Brain Res Dev Brain Res. 57:269–277.
Merkle FT, Mirzadeh Z, Alvarez-Buylla A. 2007. Mosaic organization of neural stem cells in the adult brain. Science. 317:381–384.
Nacher J, Varea E, Blasco-Ibanez JM, Castillo-Gomez E, Crespo C, Martinez-Guijarro FJ, McEwen BS. 2005. Expression of the transcription factor Pax 6 in the adult rat dentate gyrus. J Neurosci Res. 81:753–761.
Pencea V, Bingaman KD, Freedman LJ, Luskin MB. 2001. Neurogenesis in the subventricular zone and rostral migratory stream of the neonatal and adult primate forebrain. Exp Neurol. 172:1–16.
Quinones-Hinojosa A, Sanai N, Gonzalez-Perez O, Garcia-Verdugo JM. 2007. The human brain subventricular zone: stem cells in this niche and its organization. Neurosurg Clin N Am. 18:15–20vii.
Rodriguez-Perez LM, Perez-Martin M, Jimenez AJ, Fernandez-Llebrez P. 2003. Immunocytochemical characterisation of the wall of the bovine lateral ventricle. Cell Tissue Res. 314:325–335.
Sanai N, Nguyen T, Ihrie RA, Mirzadeh Z, Tsai HH, Wong M, Gupta N, Berger MS, Huang E, Garcia-Verdugo JM, et al. 2011. Corridors of migrating neurons in the human brain and their decline during infancy. Nature. 478:382–386.
Sanai N, Tramontin AD, Quinones-Hinojosa A, Barbaro NM, Gupta N, Kunwar S, Lawton MT, McDermott MW, Parsa AT, Manuel-Garcia Verdugo J, et al. 2004. Unique astrocyte ribbon in adult human brain contains neural stem cells but lacks chain migration. Nature. 427:740–744.
Sasaki E, Suemizu H, Shimada A, Hanazawa K, Oiwa R, Kamioka M, Tomioka I, Sotomaru Y, Hirakawa R, Eto T, et al. 2009. Generation of transgenic non-human primates with germline transmission. Nature. 459:523–527.
Sawamoto K, Hirota Y, Alfaro-Cervello C, Soriano-Navarro M, He X, Hayakawa-Yano Y, Yamada M, Hikishima K, Tabata H, Iwanami A, et al. 2011. Cellular composition and organization of the subventricular zone and rostral migratory stream in the adult and neonatal common marmoset brain. J Comp Neurol. 519:690–713.
Sawamoto K, Wichterle H, Gonzalez-Perez O, Cholfin JA, Yamada M, Spassky N, Murcia NS, Garcia-Verdugo JM, Marin O, Rubenstein JL, et al. 2006. New neurons follow the flow of cerebrospinal fluid in the adult brain. Science. 311:629–632.
Snapyan M, Lemasson M, Brill MS, Blais M, Massouh M, Ninkovic J, Gravel C, Berthod F, Gotz M, Barker PA, et al. 2009. Vasculature guides migrating neuronal precursors in the adult mammalian forebrain via brain-derived neurotrophic factor signaling. J Neurosci. 29:4172–4188.
Toth ZE, Mezey E. 2007. Simultaneous visualization of multiple antigens with tyramide signal amplification using antibodies from the same species. J Histochem Cytochem. 55:545–554.
Weinandy F, Ninkovic J, Gotz M. 2011. Restrictions in time and space—new insights into generation of specific neuronal subtypes in the adult mammalian brain. Eur J Neurosci. 33:1045–1054.
Whitman MC, Greer CA. 2009. Adult neurogenesis and the olfactory system. Prog Neurobiol. 89:162–175.
Winpenny E, Lebel-Potter M, Fernandez ME, Brill MS, Gotz M, Guillemot F, Raineteau O. 2011. Sequential generation of olfactory bulb Glutamatergic neurons by Neurog2-expressing precursor cells. Neural Dev. 6:1–18.
Young KM, Fogarty M, Kessaris N, Richardson WD. 2007. Subventricular zone stem cells are heterogeneous with respect to their embryonic origins and neurogenic fates in the adult olfactory bulb. J Neurosci. 27:8286–8296.